Magnetic fraction of the atmospheric dust in Kraków – physicochemical characteristics and possible environmental impact

Jan M. Michalik[1], Wanda Wilczyńska-Michalik[2], Łukasz Gondek[1], Waldemar Tokarz[1], Jan Żukrowski[3], Marta Gajewska[3], Marek Michalik[4]

[1] AGH University of Science and Technology, Faculty of Physics and Applied Computer Science, Department of Solid State Physics, A. Mickiewicza Av. 30, 30-059 Krakow, Poland;
[2] Pedagogical University, Institute of Geography, ul. Podchorążych 2, 30-084 Kraków, Poland;
[3] AGH University of Science and Technology, Academic Centre for Materials and Nanotechnology, A. Mickiewicza Av. 30, 30-059 Kraków, Poland;
[4] Jagiellonian University, Institute of Geological Sciences, ul. Gronostajowa 3a, 30-387 Kraków, Poland

Correspondence to: Jan M. Michalik (jmichali@agh.edu.pl)

Abstract. Magnetic fraction of the atmospheric dust was collected in Kraków using a static sampler and analysed using several methods (scanning electron microscopy with energy dispersive spectrometry, transmission electron microscopy with energy dispersive spectrometry, X-ray diffraction, Mössbauer spectrometry, and vibrating sample magnetometer (VSM) measurements). The magnetic fraction contains magnetite, hematite and α-Fe, as well as quartz, feldspar and pyroxene. The magnetic particles vary in size from above 20 μm to nanoparticles below 100 nm, as well as in morphology (irregular or spherical). Their chemical composition is dominated by Fe, often with Mn, Zn, Cr, Cu, Si, Al, S, Ca and other elements. Mössbauer spectroscopy corroborates the composition of the material, giving further indication of smaller than 100 nm particles present in the atmospheric dust. VSM measurements confirm that the strength of the magnetic signal can be treated as a meter of the anthropogenic impact on the suspended particulate matter, once again highlighting the presence of nanoparticles.

1 Introduction

Magnetic fraction of atmospheric dust can be considered as a main carrier of metals, especially Fe and transition metals. Usually, the magnetic properties of the total particulate matter samples (e.g. PM10, PM2.5, PM1) are analysed (Górka-Kostrubiec et al., 2020; Morris et al., 1995; Muxworthy et al., 2003; Petrovský et al., 2013; Revuelta et al., 2014; Sagnotti et al., 2006; Spassov et al., 2004; Wang et al., 2017). Baatar et al. (2017) studied the magnetic properties of atmospheric dust removed from the atmosphere during rainfall. The magnetic characteristics of the atmospheric particulate matter is sometimes studied using dust fall samples (e.g. Liu et al. 2019; Magiera et al. 2010). The magnetic properties of particles deposited on biological surfaces can be useful in terms of the biomagnetic monitoring of atmospheric pollution (Hofman et al., 2017; Maher, 2009; Mejía-Echeverry et al., 2018). Rutkowski et al. (2020) studied the magnetic parameters of dust deposited on spider webs.

Magnetic fraction of the atmospheric particulate matter is rarely collected separately using specially constructed samplers (Cheng et al., 2018, 2014; Wirth and Prodi, 1972). Magnetic fraction collected separately, even containing an admixture of non-magnetic particles, allows more precise characterisation of magnetic particles compared with total particulate matter sample (e.g. PM10).

35 Zhang et al. (2020), determined (after extraction from PM2.5 samples) an annual mean concentration of magnetite nanoparticles in urban atmosphere in Beijing to be 75.5 ± 33.2 ng m^{-3} and daily intake of magnetite was estimated to be 16.6 ± 7.3, 29.5 ± 13, and 36.4 ± 16 ng kg^{-1} of body weight (bw) per day for adults, children, and toddlers respectively. For outdoor professions intake value can reach up to 42 ng kg^{-1} bw day^{-1}.

Metal-containing particles are hazardous for human health (e.g., Sorensen, 2005; Zhang et al. 2020). The toxicity of metallic
40 particles is related among others, to the oxidative stress. The effect is significant for transition metal-containing particles because of Haber–Weiss and Fenton-type reactions (Biswas and Wu, 2005; Manke et al., 2013). Morris et al. (1995) proved the correlation between magnetic susceptibility and the mutagenicity of organic extracts from filters containing PM10 particulate matter. Maher et al. (2016) proved that magnetite nanoparticles present in the human brain are of airborne origin. Magnetite pollution nanoparticles may constitute a risk factor for Alzheimer's and Parkinson's diseases (Calderón-
45 Garcidueñas et al., 2019; Gonet and Maher, 2019; Maher, 2019). Calderón-Garcidueñas et al. (2019) identified combustion- and friction-derived iron-rich, strongly magnetic nanoparticles in the hearts of residents of polluted cities. Lu et al. (2020) identified exogenous nanoparticles containing Fe and other transition metals and metalloids in human serum and pleural effusion.

Metals (e.g. Fe, Ti, Mn) in aerosol particles are active in the catalytic oxidation of SO2 in the atmosphere and formation of
50 sulphate aerosol (Alexander et al., 2009; Dupart et al., 2012) Dust acts as a carrier of nutrients (e.g. Fe, P) transported to aquatic environments (Baker et al., 2006; Buck et al., 2010) and consequently can modify processes in the biosphere by providing various elements (e.g. Zn, Cu, Mn) (e.g., Mackey et al., 2015; Mahowald et al., 2018; Paytan et al., 2009). Fe-rich particles are commonly dark coloured and participate in the heating effect in the atmosphere (Moteki et al., 2017). It was evaluated that Fe oxide aggregated magnetite nanoparticles from anthropogenic sources contribute to 4–7 % of the shortwave absorption of
55 black carbon (Ito et al., 2018).

2. Methods

2.1 Magnetic fraction collection

To collect the magnetic fraction of atmospheric dust, a static (passive) sampler composed of a matrix of solid magnets arranged to increase gradients and magnetic field strength was used (Fig. 1A, B, C). It was covered with a 25 μm thick PVC film in
60 order to ease the separation of the collected sample from the sampler itself. After nine months of exposition, the surfaces of the sampler were covered with a thin and uneven layer of dust (Fig. 1D). The sampling site was situated at the III Campus of

Jagiellonian University (Gronostajowa Street, Kraków, Poland). Two double collecting surfaces were situated vertically ca. 1.5–1.7 m above the surface of ground covered by grass.
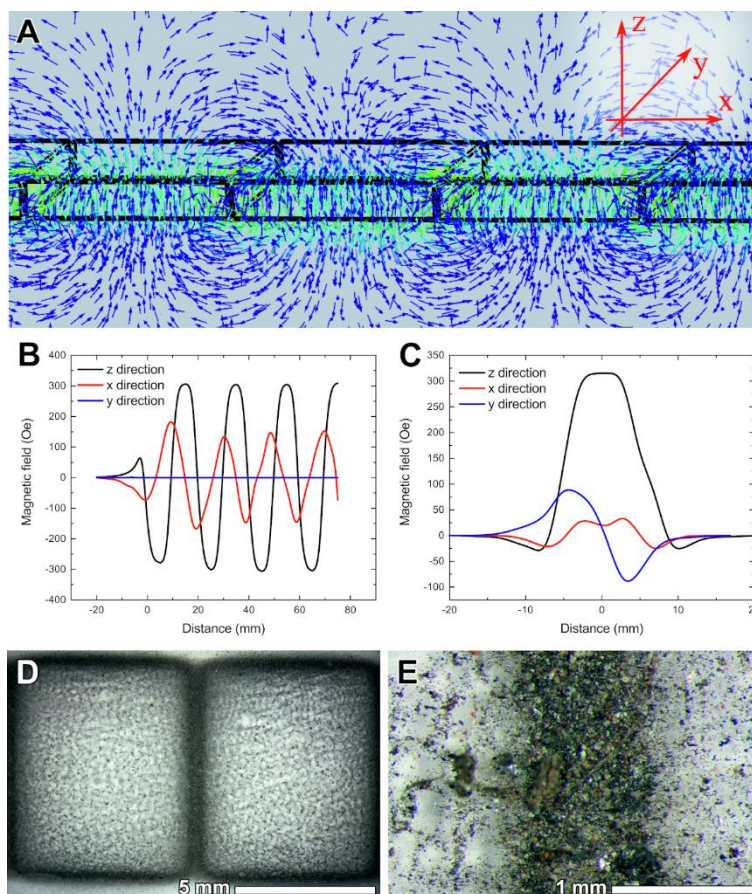
Fig. 1. A: Simulation of magnetic field induction vector direction along a matrix of solid magnets; **B & C:** measured magnetic field intensity along the matrix of magnets (B) and in a direction perpendicular to the long axis of magnets – x, y and z directions of magnetic field as indicated. **D and E.** Magnetic fraction on the passive sampler; **D.** Sample on the surface of rectangular magnet covered with PVC foil; **E.** Dust grains of various colour, size and shape on the surface of the sampler.

2.2 Scanning and transmission electron microscopy with energy dispersive spectrometry

Field emission scanning electron microscope ([FE-SEM], HITACHI S-4700) equipped with X-ray energy dispersive spectrometer ([EDS], NORAN NSS) were used to study the morphology of the components of magnetic fraction and their chemical composition. Samples mounted on adhesive carbon discs were carbon coated. Both secondary electron (SE) and backscattered electron (BSE) modes were used for imaging. Accelerating voltage of 20 kV, 10 µA current and 100 s counting time were applied for the chemical analyses. The standardless method was applied for the quantification of the chemical elements. Transmission electron microscopy (TEM) investigations were carried out on a Tecnai TF20 X-TWIN FEG microscope (Thermo Fisher Scientific), equipped with an energy dispersive X-ray detector (EDAX), working at an accelerating voltage of 200 kV. Samples for the TEM observations were prepared by the drop casting of isopropyl alcohol/atmospheric

dust dispersion on carbon-coated copper TEM grids. Bright field (BF), scanning transmission electron microscopy (STEM) and high resolution transmission electron microscopy (HRTEM) observations were performed, as well as chemical (EDS) and electron diffraction (selected area electron diffraction [SAED]) analyses.

2.3 X-ray diffraction analysis

X-ray diffraction (XRD) measurements were done by means of Malvern Panalytical Empyrean powder diffractometer using Cu K_α radiation. The powdered samples were placed on single-crystalline silicon no-background holders. The measurements were performed primarily on the samples without any treatment. Unfortunately, contribution originating from SiO_2 surpasses reflections from other phases. Therefore, the samples were grounded and suspended into distilled water in the presence of a magnetic field in order to separate the magnetic fractions, which were of the main interest. This process significantly improved the chances of identifying other phases. The collected diffraction patterns were analysed in terms of the Rietveld method using the FullProf Suite Package (Rodríguez-Carvajal, 1993).

2.4 Mössbauer spectroscopy and magnetisation measurements

[57]Fe Mössbauer measurements were carried out in the transmission mode utilising a constant acceleration spectrometer using [57]Co in a rhodium matrix as a source. Low-temperature measurements were carried out in a cold finger type cryostat, filled with liquid nitrogen. The obtained spectra were fitted using the Gauss–Newton's iterative method of minimising the chi^2, with a Lorentzian shape of the spectral lines. Magnetic isothermal loops M(H) at room temperature as well as at liquid nitrogen temperature were measured in a range up to 10 kOe using the Lake Shore Vibrating Sample Magnetometer model 7300 (VSM). The temperature stability was monitored during the measurements. Zero field cooled (ZFC) and field cooled (FC) magnetic curves were measured as well.

3 Results and discussion

3.1 General description and mineral composition of the magnetic fraction

The magnetic fraction collected on the sampler surfaces is composed of grainy material of different size and colour. The dominant part of the grains is dark grey, although colourless and transparent, brown, reddish or lustrous are also present (Fig. 1E). The size of the particles observed in electron microscope varies from more than 30 μm to below 100 nm. The number of the largest particles in the sample is low, but their share is significant considering the volume or mass of these particles. Because of the relatively high content of particles larger than 10 μm, the sample differs from typical PM10 samples.

The results of the XRD studies (Fig. 2) suggest that the separated fraction is dominated by magnetite (27.9 wt%), hematite (14.8 wt%) and α-Fe (1.5 wt%) in terms of the magnetic phases. It also exhibits quartz (41.2 wt%), feldspar (10.0 wt%) and

pyroxene (4.6 wt%). Precise analysis of the profile of magnetite reflexions in the XRD pattern suggest the distribution of various elements at the Fe-sites (e.g. Cr, Mn, Co, Zn) as typical of naturally abundant ferrites (Fig. 2).
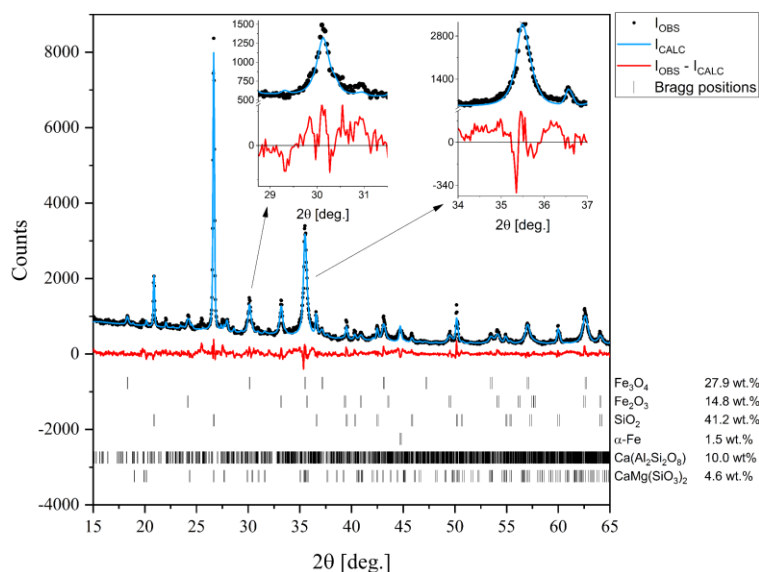

Fig. 2. X-ray diffraction pattern measured at room temperature. The black circles stand for measured data, the blue line is a theoretical spectra obtained assuming material composition as indicated, and the red line denotes the difference between the observed and measured intensities. Calculated positions of the diffraction peaks for each phase have also been indicated as bars.

Quartz grains observed using SEM are angular, different in size (with the largest up to 50 μm). Angular grains with chemical composition similar to K-feldspar and usually platy Ca sulphate crystals (possibly gypsum) were also noted using the SEM-EDS method. Relatively common are grains containing Fe, Si, Al, Ca and other elements (possibly aluminosilicates).

3.2 Form of occurrence of Fe-containing particles

Fe-containing particles analysed using the SEM-EDS method differ in size and morphology. Both irregular and spherical particles are present (Fig. 3A). The spherical particles are considered to be of anthropogenic origin and related to high temperature processes. The occurrence of natural spherical particles (cosmic, volcanic, lightning induced; e.g. Genareau et al. 2015; Genge et al., 2017) is very limited in comparison with the anthropogenic ones, but it is not possible to exclude the occurrence of spherical micrometeorites in the dust collected in urban environments (Genge et al., 2017). In the atmospheric particulate matter studied by Ebert et al. (2000) and Choël et al. (2007), most of the Fe-rich particles were spherical, that is, anthropogenic in origin. In the magnetic fraction collected in Kraków, irregular angular particles significantly prevail over spherical ones (especially in the more coarse-grained fractions), taking into account the number of particles. In the case of irregular particles, the distinction between natural and anthropogenic is difficult.
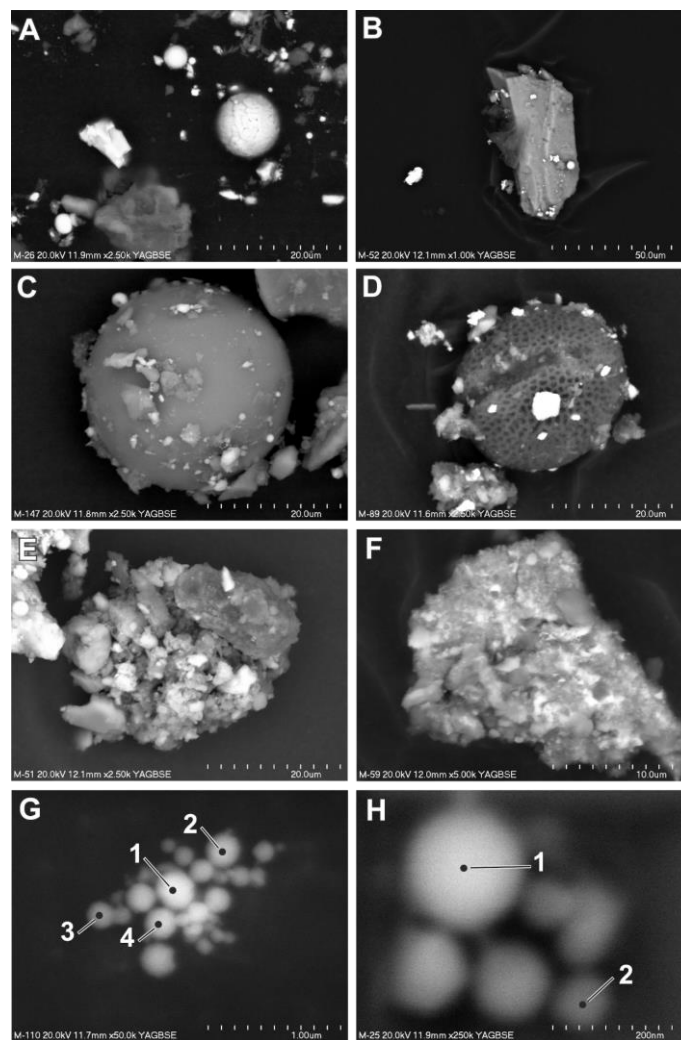
Fig. 3. Forms of occurrence of magnetic particles (SEM; backscattered electron images). A. Discrete particles of different size and shape; B. Ca-rich aluminosilicate grain with attached magnetic particles; C. Aluminosilicate sphere with attached magnetic particles; D. Pollen grain with attached magnetic particles; E. Aggregate of angular aluminosilicate grains of various chemical composition and Fe-rich particles; F. Aggregate of fine particles often with diffused boundaries; bright particles are Fe-rich; G. Aggregate composed of spherical Fe-rich particles below 200 nm in size, 1 – Fe – 60.04 wt%; Zn – 14.66 wt%; Si – 3.23 wt%; Al – 1.58 wt%; S – 3.40 wt%; Ca – 0.82 wt%; O – 16.27 wt%; 2 – Fe – 62.95 wt%; Zn – 3.59 wt%; Si – 3.13 wt%; Al – 0.90 wt%; S – 3.78 wt%; Ca – 1.17wt%; Na – 6.52 wt%; O – 17.59 wt%; 3 – Fe – 59.37 wt%; Zn – 4.41 wt%; Mn – 1.35 wt%; Si – 3.75 wt%; Al – 1.47 wt%; S – 4.93 wt%; Ca – 1.40 wt%; Na – 5.07 wt%; O – 18.24 wt%, 4 – Fe – 60.19 wt%; Zn – 11.67 wt%; Si 3.85 wt%; Al – 1.74 wt%; S – 4.04 wt%; Ca – 0.98 wt%; O – 17.53; H. Aggregate composed of spherical Fe-rich particles below 200 nm in size, 1 – Fe – 62.05 wt%; Zn – 3.95 wt%; Si – 2.83 wt%; S – 6.29 wt%; Na – 7.58 wt%; O – 17.29 wt%; 2 – Fe – 46.52 wt%; Si – 5.84 wt%; S – 13.06 wt%; Na – 14.69 wt%; O – 19.89 wt%.

Fe-containing particles occur as discrete forms of diverse size and morphology (Fig. 3A, B). Numerous Fe-containing particles occur as grains attached to the surface of larger particles (e.g. quartz, feldspar, various aluminosilicates, gypsum, spherical particles of various composition and pollen grains) (Fig. 3B–D). The number of Fe-containing particles occurring on given

6

140 larger particles is strongly variable. This form of occurrence of the atmospheric dust can be considered as an example of heterogenous clustering (Pietrodangelo et al., 2014).

Fe-containing particles also occur as a component of aggregates of various sizes and morphologies (Fig. 3E and F). The size and composition of the particles in aggregates are differentiated. Aggregates of larger particles are heterogenous (heterogenous clustering; (Pietrodangelo et al., 2014)). Homogenous aggregates (homogenous clustering; (Pietrodangelo et al., 2014)) are

145 usually composed of small (below 200 nm) Fe-rich spheres (Fig. 3G and H). Magnetic Fe-containing particles attached to larger grains or present in aggregates causes the accumulation of quartz, feldspars and other non-magnetic components in the magnetic fraction, as evidenced by XRD.

3.3 Size, morphology and chemical composition of Fe-rich particles

The Fe-containing particles vary in size from above 20 μm (rarely) (Fig. 4A and B) to nanoparticles below 100 nm (Fig. 3G,

150 3H). The particles are irregular in shape, sometimes angular, or spherical (Fig.3A, 4A - D). The content of the spherical particles in fractions above 10, 10–5, 5–2.5 and 2.5–1 μm is variable and significantly lower than the irregular ones. In the fraction below 1 μm, the number of spherical particles (53 %) slightly dominates the irregular. The results of the chemical analyses of 278 Fe-containing particles indicate that the Fe content varies from 2.32 wt% to 98.18 wt%. Particles with lower content of Fe are usually enriched in Si and Al. For some of them, the chemical composition corresponds to pyroxenes

155 determined using XRD analysis. Trace elements (content below 0.1wt%) noted in single particles are not discussed because of the low statistical value of these results.

Numerous irregular Fe-based particles contain Mn (up to 11 wt%), Cr (up to 28 wt%), Zn (up to 19 wt%), and Cu (up to 7.5 wt%) (Fig. 4H). Ni (up to 8 wt%) occurs rarely, and exclusively in particles containing Cr. W and V occur rarely in the irregular Fe-rich particles, usually in low amounts (W up to 5.45 wt%, V up to 0.76 wt%). Sb and Sn were noted only in a few particles

160 (up to ca. 1.5 wt%). Determination of the origin of the Fe-containing particles is difficult. According to Bogacki et al. (2018) re-entrained road dust contribute to 25 % in winter and 50 % in summer of the PM10 in the air in selected streets in the centre of Krakow. It indicates that long-lasting, multi-stage evolution and mixing of atmospheric particulate is possible. The form of occurrence (irregular) can be related both to natural sources (e.g. soils and the disintegration of rocks) or anthropogenic ones (e.g. metallurgical industry, fuel combustion, other industrial sectors, and traffic-related sources (exhaust and non-exhaust
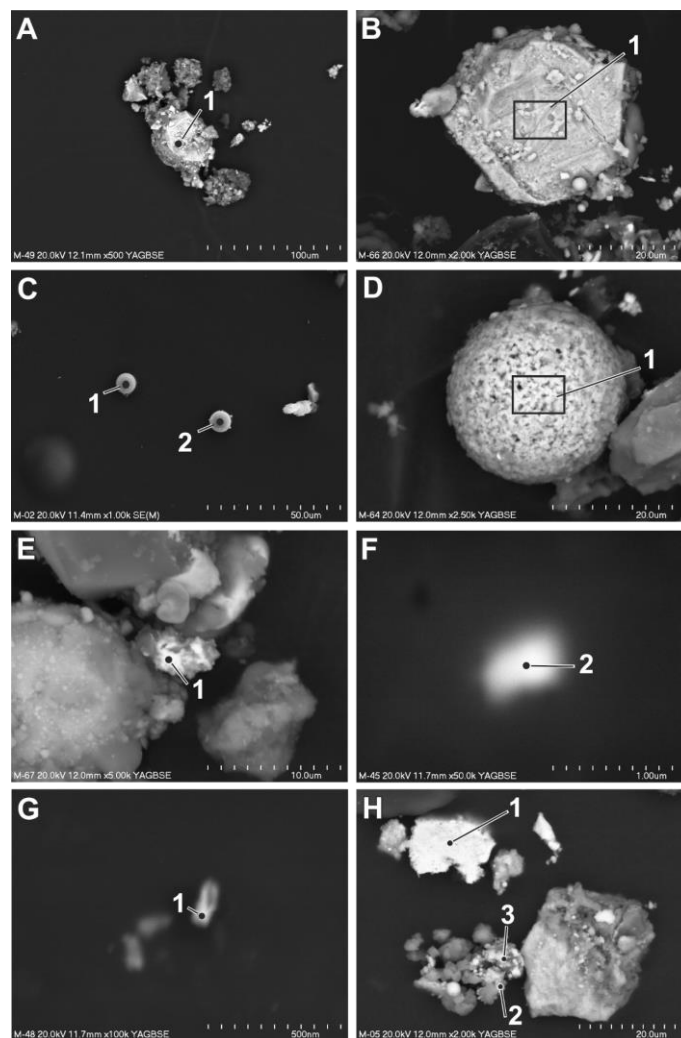
165 emissions).

Fig. 4. Size and morphology of Fe-rich particles and particles dominated by other than Fe metals or with high content other elements (SEM; backscattered electron images except C – secondary electrons). A. Irregular particles bigger than 20 μm; B. Irregular particles bigger than 20 μm; 1 – Fe – 91.33 wt%; Mn – 0.46 wt%; Si – 0.56 wt%; Ca – 0.53 wt%; O – 7.12 wt%; C. Aluminosilicate sphere (left) and Fe-dominated sphere (right); D. Spherical particle rich in Ca and Fe; 1 Fe 40.02 wt%; Ca – 35.57 wt%; Mn – 2.89 wt%; Zn – 1.47 wt%; Ti – 0.70 wt%; Si – 2.32 wt%; Al – 1.95 wt%; P – 0.13 wt%; Mg – 0.31 wt%; S – 0.15 wt%; Cl – 0.13 wt% O – 14.37 wt%; E. Particle rich in Pb; 1 - Pb – 70.25 wt%; Fe – 3.74 wt%; W – 2.31 wt%; O – 11.89 wt%; S – 10.32 wt%; Ca – 1.49 wt%; F. Particle rich in Zr; 1 - Zr – 73.08 wt%; S – 3.64 wt%; O – 21.41 wt%; Na – 1.87 wt%; G. Particle rich in Au; 1 - Au – 85.71 wt%; Na – 10.24 wt%; Si – 4.05 wt%); H. Particles with high content of other than Fe metals; 1 – Fe 68.34 wt%; Cr – 2.44 wt%; Ni – 6.33 wt%; Mn – 5.74 wt%; Si – 3.34 wt%; Al – 0.22 wt%; Ca – 0.38 wt%; S – 0.49 wt%; O – 2.72 wt%; 2 – Fe – 55.54 wt%; Zn – 13.57 wt%; Mn – 4.15 wt%; Cr – 0.85 wt%; Si – 4.02 wt%; Al – 2.31 wt%; Ca – 2.62 wt%; Mg – 1.55 wt%; S – 2.20 wt%; O – 12.85 wt%; 3 – Fe – 44.75 wt%; Zn – 19.70 wt%; Mn – 8.56 wt%; Cr – 1.26 wt%; Ni - 1.08 wt%; Ti – 0.16 wt%; Si – 2.78 wt%; Al – 0.97 wt%; Ca – 3.37 wt%; Mg – 2.91 wt%; S – 1.19 wt%; Cl – 0.39 wt%; O – 12.66 wt%.

According to Li et al. 2021 iron and steel production is a main source of magnetic particles emission and emission from power plants is on the second position. It can be assumed that in the case of the studied irregular particles natural origin is less probable, especially for the larger particles where the range of transportation in the atmosphere is limited. However, taking

8

into account their abundance in the atmospheric particulate matter samples and the scarcity of their possible natural sources in the study area, it is possible to assume that the dominant part is of anthropogenic origin. Chemical composition can be considered as an important indication of the origin of Fe-rich airborne particles (cf. Wilczyńska-Michalik et al., 2020a). It is often assumed that anthropogenic Fe-rich particles are mostly spherical (e.g., Choël et al., 2007). It is the common form originating from high temperature processes, but in iron metallurgy dust of different shape, size and chemical composition can be emitted (Jarzębski and Kapała, 1975; Wilczyńska-Michalik 1981; Jabłońska et al. 2021). In 1979 Steelworks in Krakow alone emitted dust containing 18 000 tons of Fe (Cole 1991). In 1985 emission of Fe in dust in Krakow region was estimated to be 14 000 t (Helios Rybicka 1996). Recently the emission of Fe-rich dust iron metallurgy is significantly lower but still this emission is present. It is also possible to assume that irregular Fe-containing particles are derived from fragmented metallurgical slags that are variable in chemical and mineral composition, but often contain Fe-rich components (Neuhold et al., 2019; Potysz and Kierczak, 2019), and also Cr and Mn (Horckmans et al., 2019). Metallurgical slags are often used as a substitute of natural aggregate (Horckmans et al., 2019), which could be a reason for the broad dispersion of slag-derived dust in the atmosphere. Irregular Fe-rich particles are also related to rail transportation (Moreno et al., 2015). Most of the Fe-rich particles described in the literature from this source are composed of hematite. The sampling site was situated ca. 250 m from two tram stops, which indicates that this source could also contribute to the collected magnetic fraction. Fe-rich particles occur commonly in road dust and their origin can be related to non-exhaust traffic emissions such as brake-wear emission (Grigoratos and Martini, 2015).

Several types of spherical Fe-rich particles were noted in the magnetic fraction (Fig. 4C). Aluminosilicate spheres containing usually 5–20 wt% of Fe occur rarely (Fig. 4C). Production of energy in coal-fired power plants can be considered as the main source of particulate matter of this type (Wilczyńska-Michalik et al. 2020b). Spherical forms with Fe content within the range of 35–60 wt% and Si in the 15–35 wt% range are not numerous. Only one Fe-rich spherical particle with relatively high content of Ca (possibly calcium ferrite) was noticed (Fig. 4D). Oxides of Fe_xO_y type strongly dominate the group of spherical particles. Most of these particles can be attributed to the industrial metallurgical processes (e.g., Choël et al., 2007). Spherical particles containing Cr are rare. Zn is also rare in the Fe oxide spherical particles of diameter larger than 1 μm.

Most of the spherical particles below 1 μm contain Zn (up to 27.8 wt%) (Fig. 3G, 3H). This can be related to the deposition of Zn on the surfaces of small particles during the cooling of volatile substances from metallurgical processes (Ebert et al., 2000). Mn is also a common element in Fe-rich spherical particles below 1 μm in diameter, with the highest content around 10 wt%. Cr occurs relatively rarely in this group of spherical particles. Spherical particles below 200 nm are relatively common in the group of particles below 1 μm. Spherical Fe-rich particles of diameter below 1 μm are formed commonly in metallurgical processes (Jenkins, 2003; Jenkins and Eagar, 2005). Spherical Fe nanoparticles derived from the in-cylinder melting of metallic engine parts contain Mn and Cr (Liati et al., 2015). Rail transport was recognised as a possible source of spherical nanoparticle aggregates composed of magnetite (Moreno et al., 2015). Spherical forms of 500 nm usually occur in clusters.
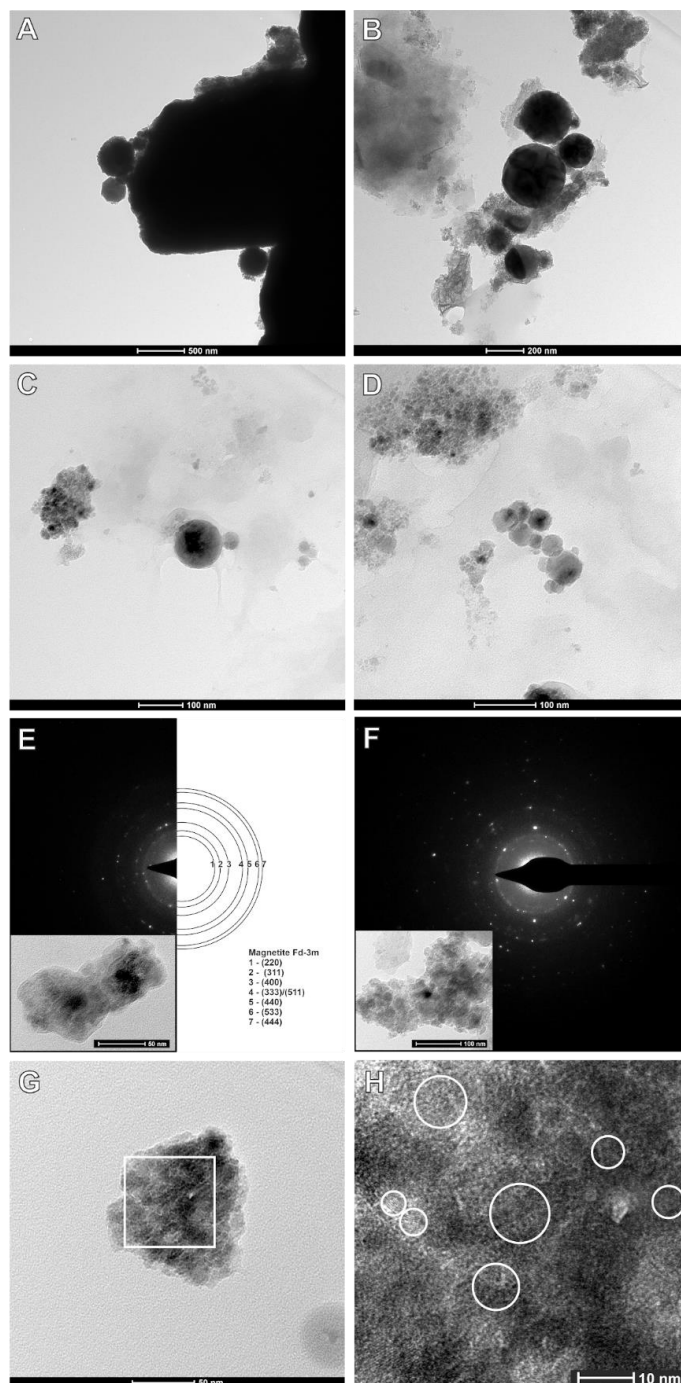
215   **Fig. 5. Fe- rich particle (TEM studies). A. Large spherical and irregular particles rich in Fe; B, C and D. Spherical particles of various size rich in Fe; E and F. SAED analyses of aggregates of irregular Fe rich particles (particles shown in insets); G. Aggregate of Fe rich particles. White square – area of HRTEM analysis. H. HRTEM analysis; white circles - domains with visible magnetite ordering.**

220 In the magnetic fraction particles with high content of other metals or dominated by other than Fe metals occur rarely (Fig. 4E, F, G, H). A few particles rich in Pb were noted (up to 70 wt%) (Fig. 4E). Three irregular particles below 1 μm in size devoid of Fe and composed predominately of Zr and O (two particles) (Fig. 4F) or Au (Fig. 4G) were analysed.

S is commonly noted in the studied Fe-rich particles and is often accompanied by Na (Fig. 3H), Cl, K, Ca, Mg and Ba. It was noted by Ito et al. (2018) that Fe in aged fly ashes is coated by Fe sulphates. According to Li et al. (2016), atmospheric metal

225 particles are internally mixed with secondary sulphates or other components.

A few particles are relatively rich in S and Fe, but without any measured O content that can indicate the presence of sulphide component.

TEM investigations were aimed at the characterisation of the smallest fraction of the analysed atmospheric dust samples. Figure 5 presents examples of bright field TEM images of the studied material. The observed particles vary widely in size and

230 shape. The smallest observed particulates are well below 10 nm in size, with the large ones exceeding a few hundred nanometres. Irregular morphology is predominant regardless of the particle size (Fig. 5A, E, F, G). Nevertheless, spherical particles of 50–200 nm diameter were also observed (Fig. 5A, B, C, D). Most of the particles analysed using EDS are rich in Fe and O, while some of them also contain Si, Zn, Mn, Al or Mg.

Selected area electron diffraction (SAED) collected from an agglomerate of the smallest fraction particles (Fig. 5E, F) allowed

235 the determination of a presence of magnetite (JCPDS card no. 00-001-1111), which is consistent with the performed XRD analysis. Domains with the magnetite ordering reach the size of 10 nm (Fig. 5G, H).

3.4 Mössbauer spectroscopy

Experimental data collected at room temperature and at 80K were fitted using doublet and sextet components (Fig. 6) based on the samples' composition obtained on the basis of XRD and chemical analysis, as well as the available literature data. For

240 the analysis of the results isomer shift (IS), quadrupole splitting ([QS], defined as half of the distance between the doublet peaks in our fits) and hyperfine magnetic field (B) values were used, together with the relative intensity (rel. int.) of each component. One has to keep in mind that in the case of the material under investigation, we cannot discard the possibility of the particles being of non-stoichiometric composition, having a large number of defects and finally their surfaces being affected by atmospheric conditions.

245 At room temperature, satisfactory results are obtained using two doublet contributions and three magnetically split sextets. The former ones are attributed to $(Ca,Mg,Fe)(SiO_3)_2$ (20.3 %) and to a collapsed spectra of FeO_x (32.2 %). Sextet due to a hyperfine magnetic field can be ascribed to a presence of α-Fe_2O_3 (18.9 %), large Fe_3O_4 (32.4 %) grains and larger particles, as well as FeX alloy (5.3 %). Low temperature measurements further support our predictions made on the basis of the room temperature measurements showing again two quadrupole split contributions: $(Ca,Mg,Fe)(SiO_3)_2$ (20.2 %) and

250 superparamagnetic iron/iron oxide particles. Three magnetically split components are again related to FeX alloy 7.4 %), α-Fe_2O_3 (10.1 %) and Fe_3O_4 grains (35.6 %) . As can be seen in Table 1, the contribution from Fe_3O_4 changes from two to four sextets. This is due to the fact that in Fe_3O_4, the iron is situated in the two crystallographically inequivalent tetrahedral (T) and

octahedral (O) sites (Tong et al., 2001). Therefore, the spectrum of Fe_3O_4 at room temperature (well above the Verwey transition – 120K) is composed of only two sextets corresponding to Fe^{3+} cations on a T site, and to Fe^{2+}/Fe^{3+} cations on an O

255   site. Below 120K, the relaxation time is extended and consequently, the O sites occupied by Fe^{2+} and Fe^{3+} can be differentiated (Řezníček et al., 2017).
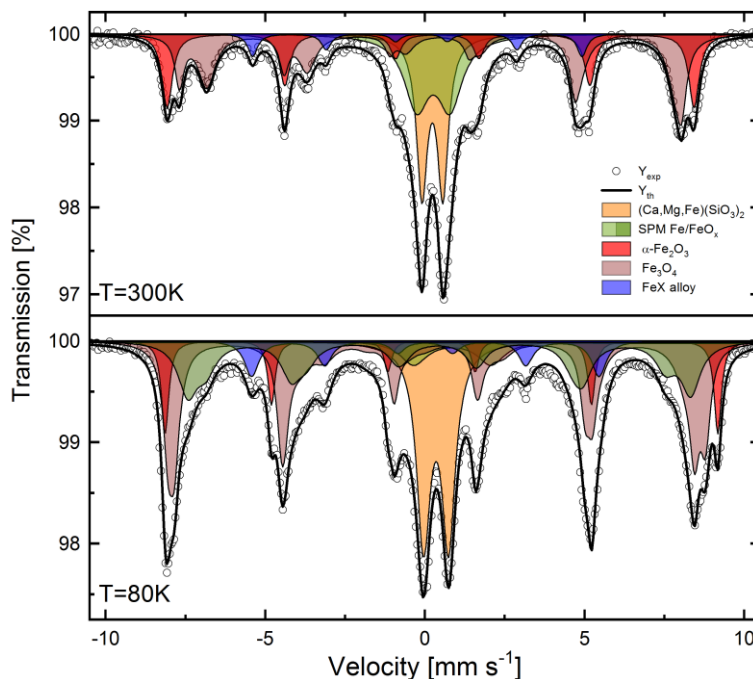

Fig. 6. Mössbauer spectra measured at room temperature (top) and at 80K (bottom). For detailed explanation and the hyperfine interaction parameter of the components used for fitting the spectra, see the text and Table 1.

260   Interestingly the contribution of the superparamagnetic grains is significantly diminished (falling from 24 % at room temperature to less than 5% at 80K). At the expense of the doublet component, a new magnetically split contribution arises related to tiny Fe_3O_4-like particles giving about 22 % of the spectra. Such behaviour of the Mössbauer spectrum typically belongs to nanosized ferromagnetic or antiferromagnetic particles. Such grains/particles (of the sizes below a single domain boundary) will present reduced hyperfine fields owing to spin relaxation effects (Yamada and Nishida, 2019). Our Mössbauer

265   spectroscopy results indicate that iron bearing particles in the aerosols are very small, showing a superparamagnetic behaviour at room temperature (RT) and becoming ferromagnetic while lowering the measurement temperature. On one hand, a possibility of superparamagnetic particles being present in the suspended particulate matter was discarded by some authors on the basis of the magnetisation measurements (Magiera et al., 2021). On the other, the possibility of the long-range transportation of tiny (a few nanometres to a few tenths of a nanometre in diameter) particles far from the industrial sources

270   cannot be eliminated. Moreover, such particles will not only travel over large distance, but also stay suspended for a long time. Bearing in mind the construction of our sample-collection device, we assume that there is a great probability of fine magnetite

particles being present in our samples. Our results are also in agreement with those presented by other groups studying aerosols and suspended particulate matter (Fu et al., 2012; Muxworthy et al., 2003).

A presence of some amount of aluminosilicates cannot be discarded based on the existence of a small component that is not

275   magnetically split down to 80K; however, the IS values do not fully support this statement, at least for ideal chemical composition and crystalline structure.

Table 1. Hyperfine interactions parameters (isomer shift, quadrupole splitting, hyperfine magnetic field) and relative component contribution for samples measured at room temperature (300K) and low temperature (80K) (IS with respect to metallic Iron at
280   **300K).**

Component	Temperature [K]	Rel. Contr. [%]	IS [mm/s]	B [kGs]	QS [mm/s]
$\alpha\text{-Fe}_2\text{O}_3$	300	18.9	0.389	511.4	-0.105
	80	10.1	0.4678	536,4	0.156
Fe_3O_4	300	32.4	0.264	487.5	0.018
			0.645	455.4	-0.026
	80	35.6	0.479	521.5	0
			0.4082	504.8	0
			0.5446	496.1	-0.325
			0.978	393.0	1.219
FeX alloy	300	5.3	-0.065	319.6	-0.067
	80	7.4	0.1179	337.1	0
$(\text{Ca,Mg,Fe})(\text{SiO}_3)_2$	300	20.3	0.341		0.327
	80	20.2	0.4549		0.393
SPM Fe/FeO$_x$	300	20.3	0.369		0.522
		2.9	1. 258		0.35
	80	22	0.518	488.1	0.037
			0.5096	446.0	-0.060
		4.7	0.9662		1.212

We are also aware of the possibility of Fe^{3+}/Fe^{2+} glasses to be used for Mössbauer spectra interpretation in the case of coal combustion products (Huffman et al., 1981; Murad and Cashion, 2004). These are commonly found in ashes from high

285   temperature processes (their content getting larger with combustion temperature rise) and are identified on the basis of the QS/IS ratio as they show a sextet collapsed into a doublet with a very broad lines. Taking into account the way we collected our samples, we would rather discard ferric or ferrous glasses from being present in the material under investigation.

3.5 Magnetisation (VSM) measurements

Magnetisation (VSM) measurements of the magnetic fraction were performed between 295 K and 77 K. The sample shows

290   typical ferromagnetic behaviour (Fig. 7). The material is almost fully saturated both at high and low temperatures. At 77 K, a wider hysteresis loop is observed as compared to the RT measurements. Unfortunately, it is not possible to estimate the size

of the nanoparticles based on the ZFC/FC experiments due to the many varieties of composition and distribution of grain size in the sample.
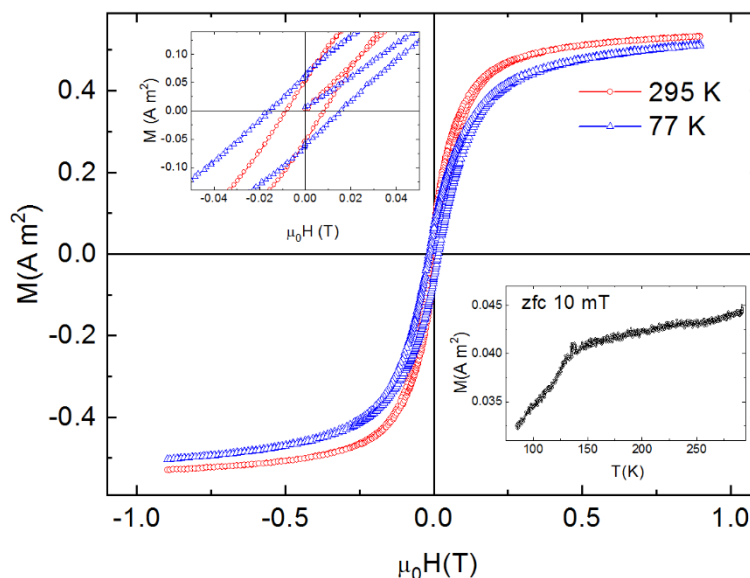
Fig. 7. Magnetic hysteresis loops up to 0.9T at room temperature (red) and at 77K (blue). Top-left inset: close-up of the area close to the zero field. Inset bottom right: ZFC curve between 300K and 77K.

In our recent contribution (Wilczyńska-Michalik et al., 2020a), we presented the results of both magnetic and Mössbauer spectroscopy studies of the soil samples from sites at different distances from industrial pollution sources. As compared to our present results, we see a great similarity to the soil samples from the polluted areas in the case of magnetisation measurements. In the case of Mössbauer spectroscopy, the situation becomes more complicated as the soil samples certainly undergo diverse processes due to oxygen exposure, humidity and so forth. However, still we observe that the fingerprints of anthropogenic particles found in our present study are clearly recognised in soils from polluted areas, in sharp contrast to soil samples from sites far from industrial plants.

4 Conclusions

- Magnetic components are present as discrete particles, as particles attached to larger grains or in aggregates of various size and composition.
- Fe-rich magnetic particles differ in morphology (irregular or spherical) and size (from above 20 μm to nanoparticles well below 100 nm). Besides Fe, other metals are also present in these particles.
- Spherical particles formed in high temperature processes are of anthropogenic origin. Most of the irregular particles are probably also of anthropogenic origin, but natural sources could also be considered.

- The abundance of spherical particles is higher among smaller particles. Spherical Fe-rich particles below 200 nm in size (often containing Zn and other metals) are a characteristic component occurring often as homogenous aggregates.

- The results of the XRD studies suggest that separated fraction is dominated by magnetite, hematite and α-Fe in terms of the magnetic phases. It also exhibits quartz, feldspar and pyroxene.

315 - Mössbauer spectroscopy indicates the presence of Fe_3O_4, α-Fe_2O_3, metallic Fe (FeX alloy) and $(Ca,Mg,Fe)(SiO_3)_2$. Clear evidence of the occurrence of nanometre scale Fe_3O_4 particles was shown.

- The study of a larger number of samples will give the possibility of better understanding the range of variability of the material as well as the health and environmental impact.

- Studying samples obtained directly at the emission sources and their comparison to our present results could give 320 indication of the impact of the particular industrial activities on the environment.

References:

330 Alexander, B., Park, R.J., Jacob, D.J., Gong, S., 2009. Transition metal-catalyzed oxidation of atmospheric sulfur: Global implications for the sulfur budget. J. Geophys. Res. 114. https://doi.org/10.1029/2008JD010486

Baatar, A., Ha, R., Yu, Y., 2017. Do rainfalls wash out anthropogenic airborne magnetic particulates? Environ. Sci. Pollut. Res. 24. https://doi.org/10.1007/s11356-017-8638-9

Baker, A.R., French, M., Linge, K.L., 2006. Trends in aerosol nutrient solubility along a west–east transect of the Saharan dust 335 plume. Geophys. Res. Lett. 33. https://doi.org/10.1029/2005GL024764

Biswas, P., Wu, C.-Y., 2005. Nanoparticles and the Environment. J. Air Waste Manage. Assoc. 55. https://doi.org/10.1080/10473289.2005.10464656

Bogacki M., Mazur M., Oleniacz R., Rzeszutek M., Szulecka A., 2018. Re-entrained road dust PM10 emission from selected streets of Krakow and its impact on air quality. Air Protection in Theory and Practice, E3S Web of Conferences 28, 01003. 340 https://doi.org/10.1051/e3sconf/20182801003

Buck, C.S., Landing, W.M., Resing, J.A., 2010. Particle size and aerosol iron solubility: A high-resolution analysis of Atlantic aerosols. Mar. Chem. 120. https://doi.org/10.1016/j.marchem.2008.11.002

Calderón-Garcidueñas, L., González-Maciel, A., Mukherjee, P.S., Reynoso-Robles, R., Pérez-Guillé, B., Gayosso-Chávez, C., Torres-Jardón, R., Cross, J. V., Ahmed, I.A.M., Karloukovski, V. V., Maher, B.A., 2019. Combustion- and friction-derived

345 magnetic air pollution nanoparticles in human hearts. Environ. Res. 176. https://doi.org/10.1016/j.envres.2019.108567

Cheng, M.-D., Allman, S.L., Ludtka, G.M., Avens, L.R., 2014. Collection of airborne particles by a high-gradient permanent magnetic method. J. Aerosol Sci. 77. https://doi.org/10.1016/j.jaerosci.2014.07.002

Cheng, M.-D., Murphy, B.L., Moon, J.-W., Lutdka, G.M., Cable-Dunlap, P.R., 2018. On the use of high-gradient magnetic force field in capturing airborne particles. J. Aerosol Sci. 120. https://doi.org/10.1016/j.jaerosci.2018.03.007

350 Choël, M., Deboudt, K., Flament, P., Aimoz, L., Mériaux, X., 2007. Single-particle analysis of atmospheric aerosols at Cape Gris-Nez, English Channel: Influence of steel works on iron apportionment. Atmos. Environ. 41. https://doi.org/10.1016/j.atmosenv.2006.11.038

Cole D. H., 1991. Cleaning Up Krakow: Poland's Ecological Crisis and the Political Economy of International Environmental Assistance. Articles by Maurer Faculty. Paper 724. http://www.repository.law.indiana.edu/facpub/724

355 Dupart, Y., King, S.M., Nekat, B., Nowak, A., Wiedensohler, A., Herrmann, H., David, G., Thomas, B., Miffre, A., Rairoux, P., D'Anna, B., George, C., 2012. Mineral dust photochemistry induces nucleation events in the presence of SO2. Proc. Natl. Acad. Sci. 109. https://doi.org/10.1073/pnas.1212297109

Ebert, M., Weinbruch, S., Hoffmann, P., Ortner, H.M., 2000. CHEMICAL CHARACTERIZATION OF NORTH SEA AEROSOL PARTICLES. J. Aerosol Sci. 31. https://doi.org/10.1016/S0021-8502(99)00549-2

360 Fu, H., Lin, J., Shang, G., Dong, W., Grassian, V.H., Carmichael, G.R., Li, Y., Chen, J., 2012. Solubility of Iron from Combustion Source Particles in Acidic Media Linked to Iron Speciation. Environ. Sci. Technol. 46. https://doi.org/10.1021/es302558m

Genareau, K., Wardman, J.B., Wilson, T.M., McNutt, S.R., Izbekov, P., 2015. Lightning-induced volcanic spherules. Geology 43. https://doi.org/10.1130/G36255.1

365 Genge, Matthew J., Davies, B., Suttle, M.D., van Ginneken, M., Tomkins, A.G., 2017. The mineralogy and petrology of I-type cosmic spherules: Implications for their sources, origins and identification in sedimentary rocks. Geochim. Cosmochim. Acta 218. https://doi.org/10.1016/j.gca.2017.09.004

Genge, M.J., Larsen, J., Van Ginneken, M., Suttle, M.D., 2017. An urban collection of modern-day large micrometeorites: Evidence for variations in the extraterrestrial dust flux through the Quaternary. Geology 45. https://doi.org/10.1130/G38352.1

370 Gonet, T., Maher, B.A., 2019. Airborne, Vehicle-Derived Fe-Bearing Nanoparticles in the Urban Environment: A Review. Environ. Sci. Technol. 53. https://doi.org/10.1021/acs.est.9b01505

Górka-Kostrubiec, B., Magiera, T., Dudzisz, K., Dytłow, S., Wawer, M., Winkler, A., 2020. Integrated Magnetic Analyses for the Discrimination of Urban and Industrial Dusts. Minerals 10. https://doi.org/10.3390/min10121056

Grigoratos, T., Martini, G., 2015. Brake wear particle emissions: a review. Environ. Sci. Pollut. Res. 22.

375 https://doi.org/10.1007/s11356-014-3696-8

Helios Rybicka E., 1996. Impact of mining and metallurgical industries on the environment in Poland. Applied Geochemistry, 11, 3-9.

Hofman, J., Maher, B.A., Muxworthy, A.R., Wuyts, K., Castanheiro, A., Samson, R., 2017. Biomagnetic Monitoring of Atmospheric Pollution: A Review of Magnetic Signatures from Biological Sensors. Environ. Sci. Technol. 51.

380 https://doi.org/10.1021/acs.est.7b00832

Horckmans, Möckel, Nielsen, Kukurugya, Vanhoof, Morillon, Algermissen, 2019. Multi-Analytical Characterization of Slags to Determine the Chromium Concentration for a Possible Re-Extraction. Minerals 9. https://doi.org/10.3390/min9100646

Huffman, G.P., Huggins, F.E., Dunmyre, G.R., 1981. Investigation of the high-temperature behaviour of coal ash in reducing and oxidizing atmospheres. Fuel 60. https://doi.org/10.1016/0016-2361(81)90158-7

385 Ito, A., Lin, G., Penner, J.E., 2018. Radiative forcing by light-absorbing aerosols of pyrogenetic iron oxides. Sci. Rep. 8. https://doi.org/10.1038/s41598-018-25756-3

Jabłońska M., Rachwał M., Wawer M., Kądziołka-Gaweł M., Teper E., Krzykawski T., Smołka-Danielowska D., 2021. Mineralogical and Chemical Specificity of Dusts Originating from Iron and Non-Ferrous Metallurgy in the Light of Their Magnetic Susceptibility. Minerals 11, 216. https://doi.org/10.3390/min11020216

390 Jarzębski S, Kapała J, 1975. Atlas zanieczyszczeń wydzielanych przy procesach hutnictwa żelaza. Wydawnictwo Śląsk. Wydawnictwo Śląsk.

Jenkins, N.T., 2003. Chemistry of Airborne Particles from Metallurgical Processing. Massachusetts Institute of Technology.

Jenkins, N.T., Eagar, T.W., 2005. Chemical Analysis of Welding Fume Particles. Suppl. To Weld. J. 87–93.

Li S., Zhang B., Wu D., Li Z., Chu S.-Q., Ding X., Tang X., Chen J., Li Q., 2021. Magnetic Particles Unintentionally Emitted

395 from Anthropogenic Sources: Iron and Steel Plants., Environ. Sci. Technol. Lett. 8, 4, 295–300. https://doi.org/10.1021/acs.estlett.1c00164

Li, W., Shao, L., Zhang, D., Ro, C.-U., Hu, M., Bi, X., Geng, H., Matsuki, A., Niu, H., Chen, J., 2016. A review of single aerosol particle studies in the atmosphere of East Asia: morphology, mixing state, source, and heterogeneous reactions. J. Clean. Prod. 112. https://doi.org/10.1016/j.jclepro.2015.04.050

400 Liati, A., Pandurangi, S.S., Boulouchos, K., Schreiber, D., Arroyo Rojas Dasilva, Y., 2015. Metal nanoparticles in diesel exhaust derived by in-cylinder melting of detached engine fragments. Atmos. Environ. 101. https://doi.org/10.1016/j.atmosenv.2014.11.014

Liu, H., Yan, Y., Chang, H., Chen, H., Liang, L., Liu, X., Qiang, X., Sun, Y., 2019. Magnetic signatures of natural and anthropogenic sources of urban dust aerosol. Atmos. Chem. Phys. 19. https://doi.org/10.5194/acp-19-731-2019

405 Lu, D., Luo, Q., Chen, R., Zhuansun Y., Jiang J., Wang W., Yang X., Zhang L., Liu X., Li F., Liu Q., Jiang G., 2020. Chemical multi-fingerprinting of exogenous ultrafine particles in human serum and pleural effusion. Nat. Commun. 11, 2567. https://doi.org/10.1038/s41467-020-16427-x

Mackey, K.R.M., Chien, C.-T., Post, A.F., Saito, M.A., Paytan, A., 2015. Rapid and gradual modes of aerosol trace metal dissolution in seawater. Front. Microbiol. 5. https://doi.org/10.3389/fmicb.2014.00794

410   Magiera T., Strzyszcz Z., Jabłońska M., Bzowska G., 2010. Characterization of magnetic particulates in urban and industrial dusts. WIT Transactions on Ecology and the Environment, 136, https://doi.org/10.2495/AIR100161

Magiera, T., Górka-Kostrubiec, B., Szumiata, T., Wawer, M., 2021. Technogenic magnetic particles from steel metallurgy and iron mining in topsoil: Indicative characteristic by magnetic parameters and Mössbauer spectra. Sci. Total Environ. 775. https://doi.org/10.1016/j.scitotenv.2021.145605

415   Maher, B.A., 2019. Airborne Magnetite- and Iron-Rich Pollution Nanoparticles: Potential Neurotoxicants and Environmental Risk Factors for Neurodegenerative Disease, Including Alzheimer's Disease. J. Alzheimer's Dis. 71. https://doi.org/10.3233/JAD-190204

Maher, B.A., 2009. Rain and Dust: Magnetic Records of Climate and Pollution. Elements 5. https://doi.org/10.2113/gselements.5.4.229

420   Maher, B.A., Ahmed, I.A.M., Karloukovski, V., MacLaren, D.A., Foulds, P.G., Allsop, D., Mann, D.M.A., Torres-Jardón, R., Calderon-Garciduenas, L., 2016. Magnetite pollution nanoparticles in the human brain. Proc. Natl. Acad. Sci. 113. https://doi.org/10.1073/pnas.1605941113

Mahowald, N.M., Hamilton, D.S., Mackey, K.R.M., Moore, J.K., Baker, A.R., Scanza, R.A., Zhang, Y., 2018. Aerosol trace metal leaching and impacts on marine microorganisms. Nat. Commun. 9. https://doi.org/10.1038/s41467-018-04970-7

425   Manke, A., Wang, L., Rojanasakul, Y., 2013. Mechanisms of Nanoparticle-Induced Oxidative Stress and Toxicity. Biomed Res. Int. 2013. https://doi.org/10.1155/2013/942916

Mejía-Echeverry, D., Chaparro, Marcos, Duque-Trujillo, J., Chaparro, Mauro, Castañeda Miranda, A., 2018. Magnetic Biomonitoring as a Tool for Assessment of Air Pollution Patterns in a Tropical Valley Using Tillandsia sp. Atmosphere (Basel). 9. https://doi.org/10.3390/atmos9070283

430   Moreno, T., Martins, V., Querol, X., Jones, T., BéruBé, K., Minguillón, M.C., Amato, F., Capdevila, M., de Miguel, E., Centelles, S., Gibbons, W., 2015. A new look at inhalable metalliferous airborne particles on rail subway platforms. Sci. Total Environ. 505. https://doi.org/10.1016/j.scitotenv.2014.10.013

Morris, W.A., Versteeg, J.K., Bryant, D.W., Legzdins, A.E., McCarry, B.E., Marvin, C.H., 1995. Preliminary comparisons between mutagenicity and magnetic susceptibility of respirable airborne particulate. Atmos. Environ. 29, 3441–3450.

435   https://doi.org/10.1016/1352-2310(95)00203-B

Moteki, N., Adachi, K., Ohata, S., Yoshida, A., Harigaya, T., Koike, M., Kondo, Y., 2017. Anthropogenic iron oxide aerosols enhance atmospheric heating. Nat. Commun. 8. https://doi.org/10.1038/ncomms15329

Murad, E., Cashion, J., 2004. Mössbauer Spectroscopy of Environmental Materials and Their Industrial Utilization. Springer US, Boston, MA. https://doi.org/10.1007/978-1-4419-9040-2

440   Muxworthy, A.R., Matzka, J., Davila, A.F., Petersen, N., 2003. Magnetic signature of daily sampled urban atmospheric particles. Atmos. Environ. 37. https://doi.org/10.1016/S1352-2310(03)00500-4

Neuhold, S., van Zomeren, A., Dijkstra, J.J., van der Sloot, H.A., Drissen, P., Algermissen, D., Mudersbach, D., Schüler, S., Griessacher, T., Raith, J.G., Pomberger, R., Vollprecht, D., 2019. Investigation of Possible Leaching Control Mechanisms for Chromium and Vanadium in Electric Arc Furnace (EAF) Slags Using Combined Experimental and Modeling Approaches.

445   Minerals 9. https://doi.org/10.3390/min9090525

Paytan, A., Mackey, K.R.M., Chen, Y., Lima, I.D., Doney, S.C., Mahowald, N., Labiosa, R., Post, A.F., 2009. Toxicity of atmospheric aerosols on marine phytoplankton. Proc. Natl. Acad. Sci. 106. https://doi.org/10.1073/pnas.0811486106

Petrovský, E., Zbořil, R., Grygar, T.M., Kotlík, B., Novák, J., Kapička, A., Grison, H., 2013. Magnetic particles in atmospheric particulate matter collected at sites with different level of air pollution. Stud. Geophys. Geod. 57.

450   https://doi.org/10.1007/s11200-013-0814-x

Pietrodangelo, A., Pareti, S., Perrino, C., 2014. Improved identification of transition metals in airborne aerosols by SEM–EDX combined backscattered and secondary electron microanalysis. Environ. Sci. Pollut. Res. 21. https://doi.org/10.1007/s11356-013-2261-1

Potysz, Kierczak, 2019. Prospective (Bio)leaching of Historical Copper Slags as an Alternative to Their Disposal. Minerals 9.

455   https://doi.org/10.3390/min9090542

Revuelta, M.A., McIntosh, G., Pey, J., Pérez, N., Querol, X., Alastuey, A., 2014. Partitioning of magnetic particles in PM10, PM2.5 and PM1 aerosols in the urban atmosphere of Barcelona (Spain). Environ. Pollut. 188. https://doi.org/10.1016/j.envpol.2014.01.025

Řezníček, R., Chlan, V., Štěpánková, H., Novák, P., Żukrowski, J., Kozłowski, A., Kąkol, Z., Tarnawski, Z., Honig, J.M.,

460   2017. Understanding the Mössbauer spectrum of magnetite below the Verwey transition: *Ab initio* calculations, simulation, and experiment. Phys. Rev. B 96. https://doi.org/10.1103/PhysRevB.96.195124

Rodríguez-Carvajal, J., 1993. Recent advances in magnetic structure determination by neutron powder diffraction. Phys. B Condens. Matter 192. https://doi.org/10.1016/0921-4526(93)90108-I

Rutkowski, R., Bihałowicz, J.S., Rachwał, M., Rogula-Kozłowska, W., Rybak, J., 2020. Magnetic Susceptibility of Spider

465   Webs and Dust: Preliminary Study in Wrocław, Poland. Minerals 10. https://doi.org/10.3390/min10111018

Sagnotti, L., Macrì, P., Egli, R., Mondino, M., 2006. Magnetic properties of atmospheric particulate matter from automatic air sampler stations in Latium (Italy): Toward a definition of magnetic fingerprints for natural and anthropogenic PM $_{10}$ sources. J. Geophys. Res. Solid Earth 111. https://doi.org/10.1029/2006JB004508

Sorensen, M., 2005. Transition Metals in Personal Samples of PM2.5 and Oxidative Stress in Human Volunteers. Cancer

470   Epidemiol. Biomarkers Prev. 14. https://doi.org/10.1158/1055-9965.EPI-04-0899

Spassov, S., Egli, R., Heller, F., Nourgaliev, D.K., Hannam, J., 2004. Magnetic quantification of urban pollution sources in atmospheric particulate matter. Geophys. J. Int. 159. https://doi.org/10.1111/j.1365-246X.2004.02438.x

Tong, Y., Li, A., Cai, Y., Ni, X., Zhang, Y., Wang, J., Guo, P., Li, X., Zhang, 2001. Mössbauer Study of Atmospheric Aerosols of Shanghai. Environ. Sci. Technol. 35. https://doi.org/10.1021/es0016497

475 Wang, J., Li, S., Li, H., Qian, X., Li, X., Liu, X., Lu, H., Wang, C., Sun, Y., 2017. Trace metals and magnetic particles in PM2.5: Magnetic identification and its implications. Sci. Rep. 7. https://doi.org/10.1038/s41598-017-08628-0

Wilczyńska-Michalik W. Mineralogical study of dusts emitted by Lenin's Steel Plant in Karków (in Polish, English summary), 1981, Prace Mineralogiczne 68, 5-52, Polska Akademia Nauk – Oddział w Krakowie, Komisja Nauk Mineralogicznych.

Wilczyńska-Michalik, W., Michalik, J.M., Kapusta, C., Michalik, M., 2020a. Airborne Magnetic Technoparticles in Soils as

480 a Record of Anthropocene. Atmosphere (Basel). 11, 44. https://doi.org/10.3390/atmos11010044

Wilczyńska-Michalik W., Dańko J., Michalik M., 2020b. Characteristics of particulate matter emitted from a coal-fired power plant. Polish Journal of Environmental Studies, 29, 2, 1411-1420. https://doi.org/10.15244/pjoes/106034

Wirth, E., Prodi, F., 1972. The concentration and size distribution of airborne ferromagnetic particles. Tellus 24. https://doi.org/10.3402/tellusa.v24i6.10683

485 Yamada, Y., Nishida, N., 2019. Iron-based Nanoparticles and Their Mössbauer Spectra. Radioisotopes 68. https://doi.org/10.3769/radioisotopes.68.125

Zhang Q., Lu D., Wang D., Yang X., Zuo P., Yang H., Fu Q., Liu Q., Jiang G., 2020. Separation and Tracing of Anthropogenic Magnetite Nanoparticles in the Urban Atmosphere. Environ. Sci. Technol. 54, 9274−9284. https://doi.org/10.1021/acs.est.0c01841